The origin of dispersion in DLA metallicities.

I. Dvorkin, J. Silk, E. Vangioni, P. Petitjean, K. A. Olive

Monthly Notices of the ROYAL ASTRONOMICAL SOCIETY

MNRAS **452,** L36–L40 (2015) doi:10.1093/mnrasl/slv085

The origin of dispersion in DLA metallicities

Irina Dvorkin,[1]★ Joseph Silk,[1,2] Elisabeth Vangioni,[1] Patrick Petitjean[1] and Keith A. Olive[3]

[1]*Sorbonne Universités, UPMC Univ Paris 6 et CNRS, UMR 7095, Institut d'Astrophysique de Paris, 98 bis bd Arago, F-75014 Paris, France*
[2]*Department of Physics and Astronomy, The Johns Hopkins University, Baltimore, MD 21218, USA*
[3]*William I. Fine Theoretical Physics Institute, School of Physics and Astronomy, University of Minnesota, Minneapolis, MN 55455, USA*

Accepted 2015 June 19. Received 2015 June 19; in original form 2015 May 15

ABSTRACT

Recent chemical abundance measurements of damped Ly α absorbers (DLAs) revealed an intrinsic scatter in their metallicity of $\sim$0.5 dex out to $z \sim 5$. In order to explore the origin of this scatter, we build a semi-analytic model which traces the chemical evolution of the interstellar matter in small regions of the Universe with different mean density, from over- to underdense regions. We show that the different histories of structure formation in these regions, namely halo abundance, mass and stellar content, are reflected in the chemical properties of the protogalaxies, and in particular of DLAs. We calculate mean metallicity–redshift relations and show that the metallicity dispersion arising from this environmental effect amounts to $\sim$0.25 dex and is an important contributor to the observed overall intrinsic scatter.

Key words: ISM: abundances – quasars: absorption lines – Galaxies: star formation.

1 INTRODUCTION

Damped Ly α absorbers (DLA), defined as quasar absorption systems with neutral column densities $N_{\rm HI} > 2 \times 10^{20}$ cm^{-2} (Wolfe et al. 1986), dominate the neutral gas content of the Universe in the redshift range $z = 0$–5 and are likely the progenitors of low-redshift galaxies (Wolfe, Gawiser & Prochaska 2005). The chemical properties of DLAs can be determined with great precision, and provide a unique probe of the properties of cold neutral gas out of which stars form at high redshifts.

Numerous surveys conducted over the past several years have provided extensive samples of high-redshift absorbers (e.g. Péroux et al. 2005; Prochaska, Herbert-Fort & Wolfe 2005; Noterdaeme et al. 2012). High-resolution observations of nearly 250 of these systems established a statistically significant decrease of DLA metallicity with increasing redshift (Prochaska et al. 2003; Rafelski et al. 2012) and a large intrinsic dispersion of $\sim$0.5 dex out to $z \sim 5$. Interestingly, this dispersion is not caused by observational uncertainties and does not appear to evolve with redshift. Neeleman et al. (2013) suggested that this effect could be partially explained by the existence of a Fundamental Plane in the redshift–mass–metallicity space, so that the dispersion in the metallicity–redshift relation is caused by the scatter in the masses of the dark matter (DM) haloes hosting the DLAs (see also Ledoux et al. 2006; Møller et al. 2013). There could be, however, additional sources of intrinsic scatter related to the environment of the galaxy or the distribution of neutral clouds within the halo.

DLAs have been extensively studied with hydrodynamic simulations (e.g. Nagamine, Springel & Hernquist 2004; Pontzen et al. 2008; Fumagalli et al. 2011; Bird et al. 2014), which have been able to reproduce the observed DLA abundance and metallicity range. While hydrodynamic simulations are becoming extremely accurate and are now able to explain many of the properties of high-redshift galaxies and their surroundings, their high computational cost prohibits studies of the large volumes of the Universe necessary for obtaining good statistics. Therefore, the study of DLA metallicity dispersion with numerical simulations is extremely challenging. Notably, Cen (2012) simulated one overdense and one underdense region, whose properties bracketed many of the observed properties of DLAs.

On the other hand, the semi-analytic approach, successfully employed in the study of galaxy evolution, enables one to reproduce large galaxy populations and perform a comprehensive parameter study at the cost of making several simplifying assumptions. Berry et al. (2014) studied DLA properties in the context of a detailed semi-analytic model of galaxy formation and were able to reproduce several key properties of DLAs, including the column density distribution and the evolution of metallicity with redshift. However, these earlier models have so far just provided mean chemical evolution trends with z.

In this work, we build a computationally efficient semi-analytic merger-tree model specifically designed to study the dispersion in the metallicity–redshift relation and the history of chemical enrichment of the Universe. We use the DM merger-tree building algorithm from the GALFORM code (Cole et al. 2000) to construct regions with different histories of structure formation. We then apply the chemical evolution model of Daigne et al. (2004, 2006) to

★ E-mail: dvorkin@iap.fr

explore the evolution of interstellar matter (ISM) metallicities in these different environments.

This Letter is organized as follows. In Section 2, we describe our model, which uses analytically computed DM halo merger trees and an accurate model of chemical evolution. In Section 3, we show that this model produces a dispersion in the observed DLA metallicities. We discuss our results in Section 4.

2 MODEL

Our goal is to calculate the dispersion in the mean mass fraction of collapsed structures, escape velocity and cosmic star formation rate (SFR) in different parts of the Universe. As a first step, we construct merger trees of DM haloes using the GALFORM algorithm (Cole et al. 2000). This algorithm relies on the extended Press–Schechter theory, in particular the conditional mass function (MF) of DM haloes, and provides a list of mergers, and the redshifts at which they occurred, that led to the formation of a given halo. The modification by Parkinson, Cole & Helly (2008) renders the algorithm consistent with the Sheth–Tormen MF (Sheth & Tormen 1999). Due to the shape of the matter power spectrum in cold DM models, the probability of a given halo with mass M_0 to merge with another halo with mass M diverges as $M \rightarrow 0$, therefore we employ a cut-off mass $M_{\rm res}$, which sets the mass resolution of our calculation. We use $M_{\rm res} = M_{\rm min}/10$ where $M_{\rm min}$ is the smallest halo mass that is able to form stars. In what follows, we explore the range $M_{\rm min} = 10^7$–$10^9\,{\rm M}_\odot\,h^{-1}$, and discuss this choice below. More details on the merger-tree building algorithm can be found in Cole et al. (2000) and Parkinson et al. (2008).

We take $V_{\rm tot} = 10^6\ ({\rm Mpc}\,h^{-1})^3$ as the total comoving volume of our calculation, having checked that for this volume, the halo MF produced with the merger-tree algorithm converges to the Sheth–Tormen MF at all redshifts, and populate it with DM haloes as follows. First, we divide the total mass range $M \in (M_{\rm res} - 10^{15}\,{\rm M}_\odot)$ into logarithmically equal bins of size $\Delta \ln M = 0.01$. We then calculate the mean number of haloes in each bin at $z = 0$ using the Sheth–Tormen MF and draw the actual number $N(M)$ from a Poisson distribution with this mean. Finally, we sample $N(M)$ haloes with logarithmically equally distributed masses in the corresponding bin.

We build a merger tree for each halo at $z = 0$ and follow its evolution backwards in time up to $z_f = 15$, saving the output in 50 redshift bins equally spaced in redshift. In this manner, we obtain the distribution of DM haloes in the comoving volume $V_{\rm tot}$ as a function of redshift. We further divide our sample into $N = 1000$ smaller *regions* $\Delta V_i = V_{\rm tot}/N = 10^3\ ({\rm Mpc}\,h^{-1})^3$ by assigning each merger tree to a random region i. This is equivalent to smoothing the density field on the scale of $r_0 \sim 10\ {\rm Mpc}\,h^{-1}$ and assuming there is no correlation between neighbouring regions. This value was chosen because on scales larger than r_0, galaxies are only weakly clustered (e.g. Norberg et al. 2001; Zehavi et al. 2005), and we expect no significant dispersion in the properties of different regions in the universe. On the other hand, for scales much smaller than r_0 there could be flow of matter between different regions so that they cannot be treated as closed boxes. In other words, here we explore the effect of dispersion on the scale of massive clusters and deep voids; further contribution is expected from galactic scales, as we briefly discuss below. For comparison, in the simulations of Cen (2012) the overdense and underdense regions had a size of roughly 20 and 30 Mpc h^{-1} on the side, respectively (see also Rollinde et al. 2013).

We then calculate the mean mass fraction in collapsed structures $f_{\rm coll}$, the mean escape velocity and the mean SFR in each region ΔV_i as explained below. While the mean MF and $f_{\rm coll}$ in our total volume $V_{\rm tot}$ coincide with the expectations from the Sheth–Thormen MF at all redshifts, their values differ in each ΔV_i region. Those regions that host a group or a cluster at low redshift have a higher concentration of structures already present at higher redshift, whereas present-day voids are relatively empty at early times. This small-scale inhomogeneity creates the observed dispersion in the different observables.

The mean mass fraction in collapsed structures $f_{\rm coll}$ is calculated by summing the masses of all the haloes above $M_{\rm min}$ in the given region and dividing by ΔV_i and the mean matter density $\rho_{\rm m}$:

$$f_{{\rm coll},i} = \frac{\sum_{M_j > M_{\rm min}} M_j}{\Delta V_i} \frac{1}{\rho_{\rm m}}\,. \quad (1)$$

The dispersion in $f_{\rm coll}$ among the different regions grows with redshift for all values of $M_{\rm min}$, reaching 0.35 dex for $M_{\rm min} = 10^9\,{\rm M}_\odot\,h^{-1}$ at $z = 10$ and 0.25 dex at $z = 5$. Furthermore, the dispersion grows with $M_{\rm min}$, since if only large structures are allowed to form, some regions remain practically devoid of structures. In the case of $M_{\rm min} = 10^8\,{\rm M}_\odot\,h^{-1}$ and $M_{\rm min} = 10^7\,{\rm M}_\odot\,h^{-1}$ the dispersion is about 0.25 dex and 0.18 dex at $z = 10$, respectively.

The mean square of the escape velocity $v_{\rm esc}^2(z)$ within each region is calculated as the mass-weighted average of $2GM/R$ for each halo mass M, where R is the virial radius enclosing a volume with mean density 200 times the critical density of the Universe. Contrary to the case of the collapse fraction, the dispersion in $v_{\rm esc}^2$ is slightly larger for smaller values of $M_{\rm min}$, being on average 0.2 dex for $M_{\rm min} = 10^7\,{\rm M}_\odot\,h^{-1}$. The reason for this is that models with low $M_{\rm min}$ exhibit a larger range of masses in each region, so that while the total mass in two representative regions might be the same, their mean escape velocities could differ substantially. In the case of high $M_{\rm min}$, however, the mass spectrum of different regions is much more uniform and the main difference is in the total mass of collapsed structures, reflected in $f_{\rm coll}$. Also contrary to the case of $f_{\rm coll}$ the dispersion in $v_{\rm esc}^2$ grows with decreasing redshift. The mean escape velocity is used in our chemical evolution code to calculate the outflow rate as explained below.

Our next step is to calculate the SFR in each halo and the mean cosmic SFR in each region ΔV_i. We use the results of Behroozi, Wechsler & Conroy (2013, hereafter B13) to calculate the SFR as a function of halo mass M and redshift z in the range $0 < z < 8$ and $9 < \log_{10}(M/{\rm M}_\odot) < 15$. We extrapolate these results to lower masses and higher redshifts with ${\rm SFR} \propto (M/{\rm M}_\odot)^\beta 10^{\alpha z}$ where $\beta = 2.1$ was obtained from a fit to the results of B13 in the range $5 < z < 8$ and $9 < \log_{10}(M/{\rm M}_\odot) < 11$ and $\alpha = -0.1$ was obtained from the observed cosmic SFR at $z \sim 10$ (Bouwens et al. 2014; Oesch et al. 2014). We note that this extrapolation is purely phenomenological and IMF (initial mass function) independent. We calculate the SFR for each halo and then compute the cosmic SFR density $\psi_i(t)$ as a function of redshift in each region ΔV_i:

$$\psi_i(t) = \frac{\sum_j {\rm SFR}(M_j, t)}{\Delta V_i}\,. \quad (2)$$

We note that by using the fit from B13 (which refers to the universal SFR density) in all of our calculations, in particular the small-scale regions, we implicitly assume that the star formation efficiency depends only on the DM halo mass and redshift. This approximation is justified by the fact that we compute mean values over sufficiently large regions, which we treat as closed boxes. The resulting dispersion in the SFR between different regions is roughly 0.4 dex, dropping significantly below $z \simeq 2.5$.

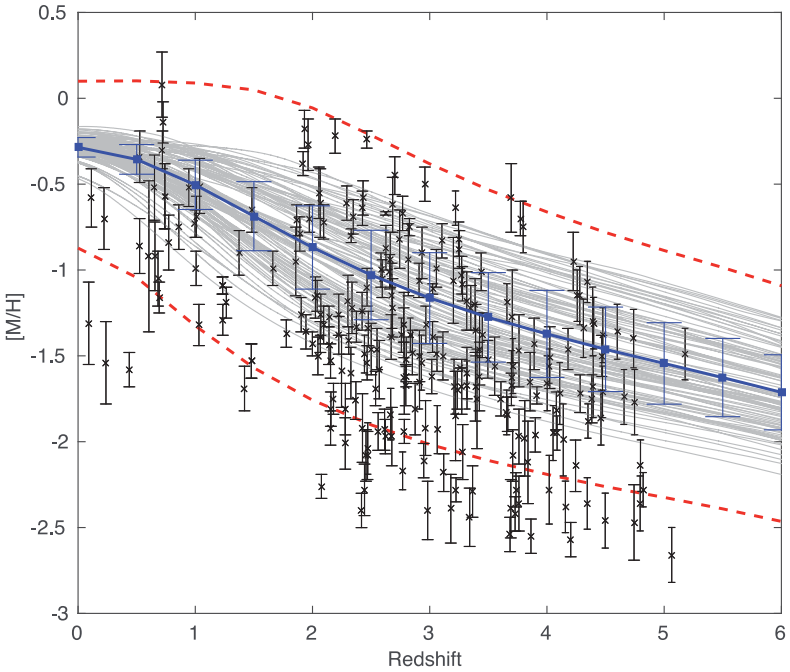

Figure 1. Log of the metallicity abundance relative to the solar value for 100 regions, each with a volume of $\Delta V_i = 10^3$ Mpc^3 h^{-3} (thin grey lines) and their mean (thick blue line) for $M_{\rm min} = 10^8\,{\rm M}_\odot\,h^{-1}$. The dispersion among the realizations and their mean is represented by the blue points with error bars. The mean dispersion in the redshift range $z = 2$–5 is 0.25 dex. Red dashed lines represent the estimated upper and lower limits when the mass–metallicity relation within each region is also considered (see text). Black points represent data from Rafelski et al. (2012).

Having obtained the rate of growth of structure and the SFR density in each region we proceed to the calculation of the chemical enrichment of the ISM. We use the chemical evolution model developed in Daigne et al. (2004, 2006) and Rollinde et al. (2009) which follows the exchange of mass between the gas within and outside of collapsed structures, the SFR at each redshift and the rate of metal production in stars.

The initial gas content of galaxies is taken to be equal to the cosmic mean $f_{\rm baryon} = \Omega_{\rm b}/\Omega_{\rm m}$. The model then follows two gas reservoirs, the intergalactic matter (IGM) and the ISM. Matter flows from IGM to ISM as the galaxies form, where baryons are assumed to follow DM, so that the mean baryon accretion rate in each region is given by $a_{\rm b}(t) = \Omega_{\rm b}{\rm d}f_{\rm coll}/{\rm d}t$ and $f_{\rm coll}$ is calculated as in equation (1). Once inside galaxies, baryons form stars according to the rate $\psi(t)$ calculated above (see equation 2). We assume a Salpeter IMF $\Phi(m)$ for $m_{\rm inf} \leq m \leq m_{\rm sup}$ with $m_{\rm inf} = 0.1\,{\rm M}_\odot$ and $m_{\rm sup} = 100\,{\rm M}_\odot$.

Baryons can flow from structures back to the IGM due to galactic winds or feedback from SNe or AGN. In this work, we consider outflows powered by stellar explosions with the rate given by

$$o(t) = \frac{2\epsilon}{v_{\rm esc}^2(t)} \int {\rm d}m \Phi(m) \Psi(t - \tau(m)) E_{\rm kin}(m), \qquad (3)$$

where $\tau(m)$ is the lifetime of a star with mass m, $E_{\rm kin}$ is the kinetic energy released when this star dies, $v_{\rm esc}$ is the mean escape velocity from structures and $\epsilon = 0.0006$ is the fraction of kinetic energy that powers the outflow. This value was chosen as in Daigne et al. (2006) through comparison of the model predictions for the IGM component and the observed oxygen and carbon abundances in the Ly α forest (e.g. Simcoe, Sargent & Rauch 2004; Songaila 2005; Aguirre et al. 2008). We verified that small deviations from this fiducial value do not have a significant effect on the resulting ISM metallicity. The contribution of this term strongly depends on $M_{\rm min}$, since small haloes have smaller escape velocities and as a result are more easily disrupted. Consequently, models with lower $M_{\rm min}$ will be able to retain fewer baryons inside the galaxies and will have lower ISM metallicities, as shown below.

To sum up, the evolution of the baryonic mass in the IGM and ISM is given by ${\rm d}M_{\rm IGM}/{\rm d}t = -a_{\rm b}(t) + o(t)$ and ${\rm d}M_{\rm ISM}/{\rm d}t = [-\psi(t) + e(t)] + [a_{\rm b}(t) - o(t)]$, where $e(t)$ is the rate at which stellar mass is returned to the ISM by mass-loss or stellar deaths. These equations are solved for each region separately, so that no matter flow is allowed between regions. This approximation is justified by our choice of the region size.

The chemical evolution of the IGM and ISM is calculated as described in Daigne et al. (2004). In particular, we do not employ the instantaneous recycling approximation but calculate the rate at which gas is returned to the ISM including the effect of stellar lifetimes and computing stellar yields for each element and for different stellar mass ranges. Further details on the chemical evolution model can be found in Daigne et al. (2004, 2006) and Vangioni et al. (2015).

In the next section, we show results for the metallicity of the ISM relative to the solar value: $[M/{\rm H}] = \log_{10}(M/{\rm H}) - \log_{10}(M/{\rm H})_\odot$ and compare it to DLA data.

3 RESULTS

We can now test our model against observational data, using DLAs as probes of the ISM at high redshift. For our fiducial model, we take $M_{\rm min} = 10^8\,{\rm M}_\odot\,h^{-1}$. We used 100 regions, each with $\Delta V_i = 10^3$ (Mpc h^{-1})^3, where both the mean and the variance (calculated in redshift bins of $\Delta z = 0.5$) over the whole ensemble converge.

In Fig. 1, we show the evolution of the metal abundance relative to the solar value for our fiducial model for 100 regions (grey lines) and compare them to observations of DLAs from Rafelski et al. (2012). The thick blue line shows the mean of all the regions and

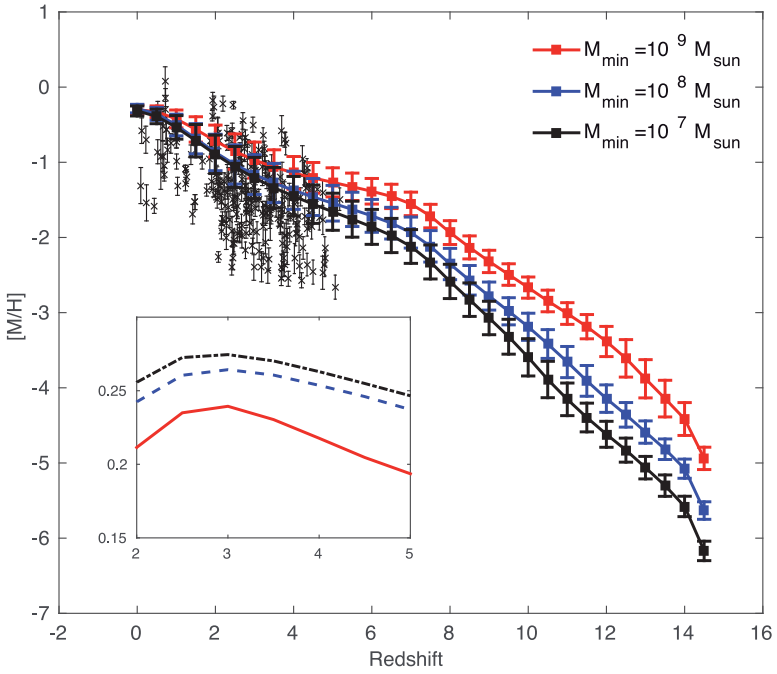

Figure 2. Log of the metallicity abundance relative to the solar value, averaged over 100 regions. Error bars show the dispersion for each model with $M_{\rm min} = 10^7$, 10^8 and 10^9 $\mathrm{M}_\odot\, h^{-1}$ (from bottom to top). Black points are measurements from Rafelski et al. (2012). The inset shows the dispersion (in dex) for $M_{\rm min} = 10^7$, 10^8 and 10^9 $\mathrm{M}_\odot\, h^{-1}$ (from top to bottom).

the error bars represent their variance. It can be seen that the dispersion predicted by the model (0.25 dex in the redshift range of the observations) is significant, but smaller than the observed dispersion in the metallicity–redshift relation (0.5 dex). We can thus conclude that the dispersion in the fraction of collapsed structures, escape velocity and SFR in each region ΔV_i contributes to the dispersion in the metallicity–redshift relation of the DLAs, but is not its only source. We note that the dispersion predicted by our model is a lower limit on the actual value, since the observed metallicity of a given DLA system might also depend on the mass of the host DM halo. Indeed, Neeleman et al. (2013) showed that by applying a correction following from the existence of a global mass–metallicity–redshift plane, the scatter in the metallicity–redshift relation reduces from 0.5 to 0.38 dex. In addition, the potential metallicity gradients of DLAs can also contribute to the dispersion (Chen et al. 2005; Christensen et al. 2014). Keeping in mind that the observational uncertainty for each measurement is about 0.12 dex, it is tempting to suggest that the combination of a mass–metallicity–redshift plane and the effect explored here, which stems mainly from the different formation epochs of structures in over- and underdense regions, might explain the observed dispersion. We stress that although we expect a correlation between these two effects, they are somewhat distinct. Indeed, the dispersion in the mean $\log M_{\rm halo}$ *between* regions is below 0.01 dex for $z < 5$.

While the modelling of the full effect is beyond the scope of this Letter, we tried to estimate it using the observed mass–metallicity relation from Maiolino et al. (2008) and the dispersion in stellar masses within each region using our merger tree, assuming for simplicity a constant stellar mass to halo mass ratio. Since the mass–metallicity relation is redshift related, and the parameters for high redshifts are somewhat uncertain (see also Zahid et al. 2013), we used the relation for $z = 3.5$ for the whole redshift range shown in Fig. 1. Adding the resulting dispersion to the metallicities calculated with our model (grey lines) produces the upper and lower limits shown as the red dashed lines in Fig. 1. It can be seen that this very rough estimate can indeed explain the whole observed range of DLA metallicities, although we caution that a more self-consistent treatment is needed, which we leave to future work.

The choice of the minimal halo mass that is able to form stars affects both the normalization and the dispersion of the predicted metallicity, as can be seen in Fig. 2, where we show model results for $M_{\rm min} = 10^7$, 10^8 and 10^9 $\mathrm{M}_\odot\, h^{-1}$ (from bottom to top). In the case of high-$M_{\rm min}$ galaxies start forming later, but they are on average more massive and have higher escape velocities. As a consequence, the outflows are weaker and a larger fraction of metals produced in stars stay in the ISM as compared to the case of low $M_{\rm min}$. It is interesting to note that the explored range $M_{\rm min} = 10^7$–10^9 $\mathrm{M}_\odot\, h^{-1}$ matches the mean of the observations. We note that the numerical simulations of Nagamine et al. (2004) show that the halo mass scale below which no DLAs exist is slightly above 10^8 $\mathrm{M}_\odot$ at $z = 3$–4, whereas Pontzen et al. (2008) find that the occurrence rate of DLAs drops sharply below $M \sim 10^9$ $\mathrm{M}_\odot$ (although see Webster, Bland-Hawthorn & Sutherland 2015). Our results are also consistent with these limits.

The inset in Fig. 2 shows the dispersion in metallicity among 100 regions as a function of redshift. It can be seen that the dispersion is larger for smaller $M_{\rm min}$. In fact, there are two competing effects: in models with larger $M_{\rm min}$, the dispersion in $f_{\rm coll}$ is larger, but the dispersion in $v_{\rm esc}^2$ is smaller. While $f_{\rm coll}$ determines the overall number of galaxies in each region, $v_{\rm esc}^2$ influences the outflow, and is particularly important in low-mass haloes which could thereby lose a substantial fraction of their newly acquired metals.

4 DISCUSSION

In this Letter, we have used the chemical evolution model of Daigne et al. (2004, 2006), supplemented by a merger-tree description of structure formation and an observation-based estimate of the SFR,

to study the metal-enrichment process of the ISM. Our models include the full range of galaxy-formation physics required to study the chemical evolution of DLAs, including gas accretion, SFRs, star formation histories, gas outflows and mergers. We reached two important conclusions.

(i) The dispersion in structure formation rates in different parts of the Universe and the accompanying variance in the stellar content of protogalaxies produces a dispersion in the metallicity–redshift relation of DLAs of roughly 0.25 dex. Furthermore, this dispersion depends on the assumed minimal mass of haloes that are able to form stars $M_{\rm min}$ through the dispersion in the structure formation histories: models with smaller $M_{\rm min}$ produce larger dispersion.

(ii) The range $M_{\rm min} = 10^7$–$10^9\,{\rm M}_\odot\,h^{-1}$ provides a good description of the data with little variance between these models. This mass range corresponds to halo masses with virial temperatures above $T \gtrsim 10^4$ for which neutral gas cooling is inefficient.

The dispersion resulting from our model is smaller than the observed value of ∼0.5 dex, but is clearly an important ingredient in the overall effect. Another potentially important source of intrinsic scatter stems from the difference in the masses of DM haloes hosting the DLAs, for example through the global mass–metallicity–redshift relation discovered by Neeleman et al. (2013). Specifically, even within each over- or underdense region, there is a certain spectrum of halo masses with different metal-enrichment histories. According to our very rough estimate, the combination of these two effects can explain the observed dispersion, but a more rigorous treatment is needed, which takes into account their possible correlations. Another important effect is related to the structure of the galactic haloes giving rise to the DLAs, which may also contribute to the observed metallicity dispersion.

Although the conclusions outlined above are relatively robust, our model involves several approximations which can be readily improved. One such assumption is the SFR as a function of halo mass and redshift, in particular our extrapolation of the results of B13 to high redshifts and low masses, down to $M = 10^7\,{\rm M}_\odot$. It would be beneficial to explore more accurate and physically motivated extrapolation schemes, for example using full semi-analytic models of galaxy evolution.

Galactic outflows obviously play an important role in galaxy evolution, and in particular in the process of metal enrichment of the ISM. We have partly addressed this issue by considering different values of $M_{\rm min}$ which resulted in different mean escape velocities and outflow rates. This effect is crucial in setting the correct metallicity normalization, and we have showed that models with lower $M_{\rm min}$ have lower mean escape velocities and retain less metals in the ISM. Clearly, a more comprehensive study of the effects of different feedback mechanisms on the normalization and dispersion in DLA metallicities is warranted, and we leave this to future work.

Finally, we plan to extend the model presented here to a full description of chemical enrichment on a halo-to-halo basis. This will allow us to address the issue of a global mass–metallicity–redshift relation of DLAs, as well as the effect of the impact parameter of quasar sightlines, thereby accounting for the different sources of metallicity dispersion.

ACKNOWLEDGEMENTS

We thank the GALFORM team for making the code publicly available. The work of ID and JS was supported by the ERC project no. 267117 (DARK) hosted by Université Pierre et Marie Curie (UPMC) – Paris 6, PI J. Silk. JS acknowledges the support of the JHU by NSF grant OIA-1124403. The work of KAO was supported in part by DOE grant DE-SC0011842 at the University of Minnesota. This work has been carried out at the ILP LABEX (under reference ANR-10-LABX-63) supported by French state funds managed by the ANR within the Investissements d'Avenir programme under reference ANR-11-IDEX-0004-02, and was also sponsored by the French Agence Nationale pour la Recherche (ANR) via the grant VACOUL (ANR-2010-Blan-0510-01).

REFERENCES

Aguirre A., Dow-Hygelund C., Schaye J., Theuns T., 2008, ApJ, 689, 851
Behroozi P. S., Wechsler R. H., Conroy C., 2013, ApJ, 770, 57 (B13)
Berry M., Somerville R. S., Haas M. R., Gawiser E., Maller A., Popping G., Trager S. C., 2014, MNRAS, 441, 939
Bird S., Vogelsberger M., Haehnelt M., Sijacki D., Genel S., Torrey P., Springel V., Hernquist L., 2014, MNRAS, 445, 2313
Bouwens R. J. et al., 2014, ApJ, 795, 126
Cen R., 2012, ApJ, 748, 121
Chen H.-W., Prochaska J. X., Weiner B. J., Mulchaey J. S., Williger G. M., 2005, ApJ, 629, L25
Christensen L., Møller P., Fynbo J. P. U., Zafar T., 2014, MNRAS, 445, 225
Cole S., Lacey C. G., Baugh C. M., Frenk C. S., 2000, MNRAS, 319, 168
Daigne F., Olive K. A., Vangioni-Flam E., Silk J., Audouze J., 2004, ApJ, 617, 693
Daigne F., Olive K. A., Silk J., Stoehr F., Vangioni E., 2006, ApJ, 647, 773
Fumagalli M., Prochaska J. X., Kasen D., Dekel A., Ceverino D., Primack J. R., 2011, MNRAS, 418, 1796
Ledoux C., Petitjean P., Fynbo J. P. U., Møller P., Srianand R., 2006, A&A, 457, 71
Maiolino R. et al., 2008, A&A, 488, 463
Møller P., Fynbo J. P. U., Ledoux C., Nilsson K. K., 2013, MNRAS, 430, 2680
Nagamine K., Springel V., Hernquist L., 2004, MNRAS, 348, 421
Neeleman M., Wolfe A. M., Prochaska J. X., Rafelski M., 2013, ApJ, 769, 54
Norberg P. et al., 2001, MNRAS, 328, 64
Noterdaeme P. et al., 2012, A&A, 547, L1
Oesch P. A. et al., 2014, ApJ, 786, 108
Parkinson H., Cole S., Helly J., 2008, MNRAS, 383, 557
Péroux C., Dessauges-Zavadsky M., D'Odorico S., Sun Kim T., McMahon R. G., 2005, MNRAS, 363, 479
Pontzen A. et al., 2008, MNRAS, 390, 1349
Prochaska J. X., Gawiser E., Wolfe A. M., Cooke J., Gelino D., 2003, ApJS, 147, 227
Prochaska J. X., Herbert-Fort S., Wolfe A. M., 2005, ApJ, 635, 123
Rafelski M., Wolfe A. M., Prochaska J. X., Neeleman M., Mendez A. J., 2012, ApJ, 755, 89
Rollinde E., Vangioni E., Maurin D., Olive K. A., Daigne F., Silk J., Vincent F. H., 2009, MNRAS, 398, 1782
Rollinde E., Theuns T., Schaye J., Pâris I., Petitjean P., 2013, MNRAS, 428, 540
Sheth R. K., Tormen G., 1999, MNRAS, 308, 119
Simcoe R. A., Sargent W. L. W., Rauch M., 2004, ApJ, 606, 92
Songaila A., 2005, AJ, 130, 1996
Vangioni E., Olive K. A., Prestegard T., Silk J., Petitjean P., Mandic V., 2015, MNRAS, 447, 2575
Webster D., Bland-Hawthorn J., Sutherland R. S., 2015, ApJ, 804, 110
Wolfe A. M., Turnshek D. A., Smith H. E., Cohen R. D., 1986, ApJS, 61, 249
Wolfe A. M., Gawiser E., Prochaska J. X., 2005, ARA&A, 43, 861
Zahid H. J., Geller M. J., Kewley L. J., Hwang H. S., Fabricant D. G., Kurtz M. J., 2013, ApJ, 771, L19
Zehavi I. et al., 2005, ApJ, 630, 1

This paper has been typeset from a TEX/LATEX file prepared by the author.